CHEMISTRY OF MATERIALS

ARTICLE

pubs.acs.org/cm

$Tl_2Hg_3Q_4$ (Q = S, Se, and Te): High-Density, Wide-Band-Gap Semiconductors†

Simon Johnsen,[‡] Sebastian C. Peter,[‡,▽] Sandy L. Nguyen,[‡] Jung-Hwan Song,[§] Hosub Jin,[§] Arthur J. Freeman,[§] and Mercouri G. Kanatzidis*[,‡]

[‡]Department of Chemistry and [§]Department of Physics and Astronomy, Northwestern University, Evanston, Illinois 60208, United States

Supporting Information

ABSTRACT: We present the synthesis, crystal structures, and physical properties of $Tl_2Hg_3Q_4$ (Q = S, Se, and Te). The incongruently melting $Tl_2Hg_3Q_4$ crystals were grown in a Tl_xQ flux. These compounds are isostructural and crystallize in a monoclinic cell with a layered structure, adopting the space group $C2/c$ with a = 11.493(2) Å, b = 6.6953(13) Å, c = 12.937(3) Å, β = 114.98(3)° for $Tl_2Hg_3S_4$, a = 11.977(2) Å, b = 6.9264(14) Å, c = 13.203(3) Å, β = 116.36(3)° for $Tl_2Hg_3Se_4$ and a = 12.648(3) Å, b = 7.3574(15) Å, c = 13.701(3) Å, β = 117.48(3)° for $Tl_2Hg_3Te_4$. The structures feature infinite chains of $[Hg_3Q_4]^{2-}$, which are linked into layers by charge balancing Tl atoms. The compounds have very high densities (>8.3 g/cm^3) with experimentally determined band gaps of 2.05, 1.57, and 0.90 eV for Q = S, Se, and Te, respectively. Using the refined crystal structures, we performed detailed band structure calculations at the density functional theory (DFT) level, using the screened-exchange local density approximation (sx-LDA). The results indicate that the compounds are semiconductors with the sulfur analog, having an indirect band gap, and the selenium and tellurium analogs, having direct energy band gaps. There is strong Hg 6*s* and Tl 6*p* orbital character in the conduction band minimum, while the valence band maximum has predominantly chalcogen *p* state character mixed in with a Tl 6*s* contribution. The band structure calculations support the experimental observation of a narrowing of the band gap in the series Q = S, Se, and Te, which results from the increasing extension of the outermost chalcogen *p* orbitals.

KEYWORDS: chalcogenide, X-ray detector, crystal growth, cadmium telluride

INTRODUCTION

Crystalline metal chalcogenides find increasingly broad applications in solar energy conversion,[1−3] thermoelectric energy conversion,[4−7] nonlinear optics,[8−11] phase change memory,[12,13] γ-ray detection,[14,15] environmental remediation,[16−20] and topological insulator research.[21−24] Consequently, there is an ongoing fundamental interest in chalcogenide materials and their structural, chemical, optical, and electronic properties. Control of these properties is critical in order to tailor these materials to specific purposes. The concept of "dimensional reduction" (DR) can bring some predictability to the structures and properties of solid-state compounds, and it has proven to be a useful tool for the solid-state chemist in understanding property trends.[25−30] The basic premise of DR is to dismantle a dense three-dimensional (3D) parent structure to consecutively lower-dimensional networks by the introduction of an additional nucleophilic, electronegative element. This results in an increase of the energy band gap as orbital overlap in certain space directions is reduced and energy band widths narrow. The dimensional reduction of the 3D compound MQ_x by the addition of A_yQ (Q = S, Se, Te) can be written as

$$mMQ_x + nA_yQ \rightarrow A_{yn}[M_mQ_{xm+n}] \quad (1)$$

In this case, Q^{2-} is the additional nucleophilic electronegative element and, typically, A is an alkaline or alkaline-earth element. For instance, the addition of A_2S (where A is an alkali-metal element) into CdS results in a series of lower-dimensional compounds, i.e., $K_2Cd_2S_3$ (three-dimensional (3D) open framework), $Na_6Cd_7S_{10}$ (3D open framework), $K_2Cd_3S_4$ (two-dimensional (2D)), K_2CdS_2 (one-dimensional (1D)), and K_6CdS_6 (zero-dimensional (0D)).[25,27,31,32] In each case, the degree of dimensionality of the metal-chalcogenide framework decreases as more A_2S is added. The chemical similarity of Tl and the alkali metals also makes DR possible with Tl_2Q. For example, all HgQ compounds crystallize in the 3D zincblende structure, with band gaps of 0 eV.[33] Here, we demonstrate that the addition of Tl_2Q into HgQ leads to the ternary compounds $Tl_2Hg_3Q_4$, with marked increases in band-gap energies, relative to HgQ.

Many binary chalcogenides have band gaps that are too narrow for applications in the visible region of the spectrum. DR can serve as a means to rationally create derivatives with targeted band gaps for various applications ranging from the infrared, visible, X-ray, and γ-ray detection.[14,34] Herein, we present the synthesis, crystal structure, electronic band structure, and electronic absorption properties of the ternary chalcogenides $Tl_2Hg_3Q_4$ (Q = S, Se, and Te). The $Tl_2Hg_3Q_4$ compounds are isostructural and exhibit an increase in band gap when going from the Te analogue to the S analogue. The phases have been previously indicated in HgQ−Tl_2Q pseudobinary phase diagrams;[35−37] however, neither crystal structures nor any physical properties have been reported. The compounds

Received: July 12, 2011
Revised: August 28, 2011
Published: September 16, 2011

Table 1. Crystal Data and Details of Structure Refinement for $Tl_2Hg_3Q_4$ (Q = S, Se, Te) at 293(2) K[a]

parameter	Value/Comment		
	Q = S	Q = Se	Q = Te
empirical formula	$Tl_2Hg_3S_4$	$Tl_2Hg_3Se_4$	$Tl_2Hg_3Te_4$
formula weight	1138.75	1326.35	1520.91
color	red	black	gray metallic
wavelength	0.71073 Å	0.71073 Å	0.71073 Å
crystal system	monoclinic	monoclinic	monoclinic
space group	$C2/c$	$C2/c$	$C2/c$
unit-cell dimensions	a = 11.493(2) Å	a = 11.977(2) Å	a = 12.648(3) Å
	b = 6.6953(13) Å	b = 6.9264(14) Å	b = 7.3574(15) Å
	c = 12.937(3) Å	c = 13.203(3) Å	c = 13.701(3) Å
	β = 114.98(3)°	β = 116.36(3)°	β = 117.48(3)°
volume	902.4(3) $Å^3$	981.4(3) $Å^3$	1131.1(4) $Å^3$
Z	4	4	4
density (calculated)	8.382 g cm^{-3}	8.977 g cm^{-3}	8.931 g cm^{-3}
absorption coefficient	87.291 mm^{-1}	94.249 mm^{-1}	79.017 mm^{-1}
$F(000)$	1864	2152	2440
crystal size	0.165 mm × 0.091 mm × 0.046 mm	0.121 mm × 0.166 mm × 0.441 mm	0.431 mm × 0.215 mm × 0.125 mm
θ range for data collection	3.47°−29.09°	3.44°−29.13°	3.31°−29.19°
index ranges	$-15 \le h \le 14$,	$-15 \le h \le 15$,	$-14 \le h \le 16$,
	$-9 \le k \le 9$,	$-9 \le k \le 9$,	$-9 \le k \le 10$,
	$-17 \le l \le 13$	$-18 \le l \le 18$	$-18 \le l \le 18$
reflections collected	3424	4214	4938
independent reflections	1132 [R_{int} = 0.0733]	1222 [R_{int} = 0.0794]	1412 [R_{int} = 0.0738]
completeness	93.8%	92.2%	92.2%
refinement method		full-matrix least-squares on F^2	
number of data/restraints/parameters	1132/0/43	1222/0/43	1412/0/43
goodness-of-fit	1.150	1.184	1.184
final R indices [$> 2\sigma(I)$]	R_{obs} = 0.0463,	R_{obs} = 0.0588,	R_{obs} = 0.0513,
	wR_{obs} = 0.1058	wR_{obs} = 0.1308	wR_{obs} = 0.0973
R indices [all data]	R_{all} = 0.0667,	R_{all} = 0.0704,	R_{all} = 0.0731,
	wR_{all} = 0.1351	wR_{all} = 0.1359	wR_{all} = 0.1032
extinction coefficient	0.00031(6)	0.000554(17)	0.00069(4)
largest diff. peak and hole	3.429 and −3.888 e $Å^{-3}$	4.674 and −4.828 e $Å^{-3}$	4.553 and −3.439 e $Å^{-3}$

[a] $R = \frac{\Sigma||F_o| - |F_c||}{\Sigma|F_o|}$, $wR = \left[\frac{\Sigma w(|F_o|^2 - |F_c|^2)^2}{\Sigma w|F_o|^4}\right]^{1/2}$, and calc $w = \frac{1}{\sigma^2(F\sigma^2) + (0.0642P)^2 + 63.4294P}$, where $P = (F_o^2 + 2F_c^2)/3$.

are incongruently melting, and we have synthesized pure samples using both Tl_xQ flux and direct combination reactions, followed by annealing. The most interesting feature of these systems is that they combine physical attributes that are unlikely to coexist, namely, very heavy elements, high specific density, and relatively wide band gaps. Because of this, they are potential candidates as X-ray and γ-ray detector materials.[34]

EXPERIMENTAL SECTION

Synthesis and Crystal Growth. Crystal growth was performed in a flux of excess Tl_2Q. The $Tl_2Hg_3Q_4$ compounds melt incongruently at 648, 691, and 728 K for the S, Se, and Te analogues, respectively. The corresponding peritectics are all located at $x \approx 0.35$, where x is given as $(HgQ)_{1-x}(Tl_2Q)_x$ and the liquidus extends to x = 0.55, 0.61, and 0.53, respectively. Consequently, x = 0.38 was used as the starting composition for all Q. *Warning: Because of the toxicity of both Tl and Hg, great care should be exerted with appropriate protective equipment in both the synthesis and handling of the $Tl_2Hg_3Q_4$ crystals.*

HgQ was synthesized using elemental mercury (Hg) (99.999%, Sigma−Aldrich) and elemental sulfur (S), selenium (Se), and tellurium (Te) (99.99%, 5N+; 99.999%, Tellurex; and 99.999%, Tellurex, respectively). In order to avoid potential explosions, because of the high vapor pressure of elemental Hg and the chalcogens at 873 K, a long quartz tube was used that extended from the middle to the exit of the furnace, thus providing a cold end for the elements to condense and re-evaporate, effectively generating a reflux within the reaction tube.

Tl, Q, and HgQ in the $(HgQ)_{0.62}(Tl_2Q)_{0.38}$ stoichiometry were sealed in an evacuated carbon-coated fused-silica tube. Over a period of 8 h, the tube was heated to 723, 723, and 773 K for the Q = S, Se, and Te samples, in that order, and then kept at this temperature for 8 h to ensure a homogeneous melt. The samples were then cooled over a period of 14 d to 473, 573, and 573 K for Q = S, Se, and Te. From these temperatures, the samples were cooled to room temperature in 8 h. The samples were sealed in a quartz ampule, along with some

dx.doi.org/10.1021/cm2019857 |Chem. Mater. 2011, 23, 4375–4383

Table 2. Atomic Coordinates and Equivalent Isotropic Displacement Parameters for $Tl_2Hg_3Q_4$ (Q = S, Se, Te) at 293(2) K[a]

label	Wyckoff position	Atomic Coordinates (× 10^4) x	y	z	occupancy	U_{eq} (× 10^3 Å^2)[b]
			$Tl_2Hg_3S_4$			
Tl	8*f*	8260(1)	9215(2)	9506(1)	1	21(1)
Hg(1)	4*e*	0	1252(2)	2500	1	20(1)
Hg(2)	8*f*	616(1)	6131(2)	1522(1)	1	18(1)
S(1)	8*f*	1787(6)	8907(7)	2566(5)	1	18(2)
S(2)	8*f*	871(5)	3527(7)	4256(5)	1	15(1)
			$Tl_2Hg_3Se_4$			
Tl	8*f*	8352(1)	9135(1)	9544(1)	1	26(1)
Hg(1)	4*e*	0	1338(1)	2500	1	25(1)
Hg(2)	8*f*	625(1)	6165(1)	1529(1)	1	26(1)
Se(1)	8*f*	1828(1)	8982(1)	2631(1)	1	15(1)
Se(2)	8*f*	972(1)	3621(1)	4309(1)	1	14(1)
			$Tl_2Hg_3Te_4$			
Tl	8*f*	8484(1)	9088(2)	9617(1)	1	42(1)
Hg(1)	4*e*	0	1381(2)	2500	1	38(1)
Hg(2)	8*f*	692(2)	6142(2)	1519(2)	1	62(1)
Te(1)	8*f*	1850(2)	9013(2)	2702(1)	1	25(1)
Te(2)	8*f*	1053(2)	3702(2)	4337(1)	1	20(1)

[a] Estimated standard deviations are given in parentheses. [b] U_{eq} is defined as one third of the trace of the orthogonalized U_{ij} tensor.

ceramic wool, and the excess flux was removed by centrifuging the hot samples at 573, 673, and 673 K, for the S, Se, and Te samples, respectively. After centrifugation, the crystals remained on top of the ceramic wool, while the excess Tl_xQ flux migrated to the bottom of the silica tube.

Samples of $Tl_2Hg_3Q_4$ were also synthesized in 2−5 g batches via direct combination reactions, using Tl_2Q and HgQ in a 1:3 stoichiometry. The starting compounds were sealed in carbon-coated tubes, which were heated to 823 K within 12 h and kept at this temperature for 2 d and then air-quenched. The samples were then annealed for 3 weeks at 623 K, from which they were slowly cooled to room temperature within 12 h.

Composition, Crystallographic, Optical, and Electrical Characterization. Quantitative microprobe analyses of $Tl_2Hg_3Q_4$ compounds were performed with a Hitachi Model S-3400 scanning electron microscopy (SEM) system that was equipped with a Princeton Gamma Tech (PGT) energy-dispersive X-ray analyzer. Data were acquired with an accelerating voltage of 20 kV and an accumulation time of 60 s. Energy-dispersive X-ray spectroscopy (EDS) was performed on visibly clean surfaces of the samples and gave atomic compositions in good agreement with the results derived from the single-crystal X-ray diffraction (XRD) refinements. The EDS compositions (normalized to $Tl_xHg_yQ_4$) are $Tl_{1.63(9)}Hg_{2.58(6)}S_{4.00(6)}$, $Tl_{2.12(9)}Hg_{3.21(8)}Se_{4.00(7)}$, and $Tl_{2.2(2)}Hg_{3.1(2)}Te_{4.00(7)}$, averaged over 3−5 different crystals for each batch. The error is given as the standard deviation on the obtained composition for the individual crystals. The extensive overlap of the S Kα lines with the Mα lines of both Tl and Hg results in an ill-determined stoichiometry for Q = S. For both the Se and Te samples, where the lines are well-resolved, the stoichiometries match the expected values within the error of measurement. Polycrystalline powders from the direct combination samples also exhibit the expected EDS stoichiometry.

Phase identity and purity of $Tl_2Hg_3Q_4$ (Q = S, Se, Te) were assessed using powder XRD experiments that were carried out using an Inel diffractometer with Cu Kα radiation. Experimental powder XRD patterns were compared to patterns calculated from the single-crystal structural refinement.

Table 3. Anisotropic Displacement Parameters for $Tl_2Hg_3Q_4$ (Q = S, Se, Te) at 293(2) K[a]

label	Anisotropic Displacement Parameters (× 10^3 Å^2)[b] U_{11}	U_{22}	U_{33}	U_{12}	U_{13}	U_{23}
			$Tl_2Hg_3S_4$			
Tl	24(1)	16(1)	22(1)	−1(1)	9(1)	2(1)
Hg(1)	28(1)	11(1)	24(1)	0	13(1)	0
Hg(2)	21(1)	10(1)	24(1)	−2(1)	10(1)	−2(1)
S(1)	19(2)	11(2)	25(3)	0(2)	10(2)	0(2)
S(2)	15(2)	14(2)	23(2)	2(2)	15(2)	−2(2)
			$Tl_2Hg_3Se_4$			
Tl	31(1)	26(1)	16(1)	−1(1)	6(1)	4(1)
Hg(1)	41(1)	15(1)	19(1)	0	14(1)	0
Hg(2)	33(1)	13(1)	26(1)	−8(1)	6(1)	−6(1)
Se(1)	19(1)	8(1)	14(1)	−2(1)	5(1)	−2(1)
Se(2)	21(1)	11(1)	8(1)	3(1)	5(1)	1(1)
			$Tl_2Hg_3Te_4$			
Tl	41(1)	43(1)	38(1)	−3(1)	13(1)	1(1)
Hg(1)	50(1)	29(1)	34(1)	0	18(1)	0
Hg(2)	59(1)	35(1)	70(1)	−24(1)	9(1)	−18(1)
Te(1)	24(1)	16(1)	28(1)	−2(1)	7(1)	−4(1)
Te(2)	20(1)	18(1)	20(1)	2(1)	6(1)	−1(1)

[a] Estimated standard deviations are given in parentheses. [b] The anisotropic displacement factor exponent takes the following form: $-2\pi^2(h^2a^{*2}U_{11} + ... + 2hka^*b^*U_{12})$.

dx.doi.org/10.1021/cm2019857 |*Chem. Mater.* 2011, 23, 4375–4383

Table 4. Selected Bond Lengths for $Tl_2Hg_3Q_4$ (Q = S, Se, Te) at 293(2) K[a]

label	distance (Å)	label	distance (Å)	label	distance (Å)
Tl−S(1)	2.940(6)	Tl−Se(1)	3.0731(9)	Tl−Te(1)	3.3153(17)
Tl−S(2)	3.030(6)	Tl−Se(2)	3.1389(9)	Tl−Te(2)	3.3394(17)
Tl−S(1)	3.153(6)	Tl−Se(1)	3.2071(10)	Tl−Te(1)	3.3699(17)
Tl−Tl	3.4422(19)	Tl−Tl	3.5968(8)	Tl−Tl	3.728(2)
Tl−Hg(2)	3.5259(16)	Tl−Hg(2)	3.4895(11)	Tl−Hg(2)	3.5460(19)
Hg(1)−S(1)	2.559(6)	Hg(1)−Se(1)	2.6740(8)	Hg(1)−Te(1)	2.8262(15)
Hg(1)−S(2)	2.562(5)	Hg(1)−Se(2)	2.6625(8)	Hg(1)−Te(2)	2.8161(14)
Hg(2)−S(2)	2.349(5)	Hg(2)−Se(2)	2.4715(8)	Hg(2)−Te(2)	2.6609(16)
Hg(2)−S(1)	2.357(5)	Hg(2)−Se(1)	2.4781(8)	Hg(2)−Te(1)	2.6538(15)
Hg(2)−S(1)	3.089(6)	Hg(2)−Se(1)	3.1326(10)	Hg(2)−Te(1)	3.193(2)

[a] Estimated standard deviations are given in parentheses.

Table 5. Selected Bond Angles for $Tl_2Hg_3Q_4$ (Q = S, Se, Te) at 293(2) K[a]

label	angle (deg)	label	angle (deg)	label	angle (deg)
S(1)−Tl-S(2)	91.28(16)	Se(1)−Tl(1)−Se(2)	90.78(3)	Te(1)−Tl-Te(2)	88.93(4)
S(1)−Tl-S(1)	76.17(9)	Se(1)−Tl(1)−Se(1)	76.72(2)	Te(1)−Tl-Te(1)	77.17(3)
S(2)−Tl-S(1)	95.06(15)	Se(2)−Tl(1)−Se(1)	94.65(3)	Te(2)−Tl-Te(1)	92.21(5)
S(1)−Hg(1)−S(1)	104.3(2)	Se(2)−Hg(1)−Se(2)	107.14(3)	Te(2)−Hg(1)−Te(2)	105.32(6)
S(1)−Hg(1)−S(2)	109.15(18)	Se(2)−Hg(1)−Se(1)	116.09(3)	Te(2)−Hg(1)−Te(1)	119.36(4)
S(1)−Hg(1)−S(2)	113.71(19)	Se(2)−Hg(1)−Se(1)	106.56(3)	Te(2)−Hg(1)−Te(1)	104.92(4)
S(2)−Hg(1)−S(2)	107.0(2)	Se(1)−Hg(1)−Se(1)	104.78(3)	Te(1)−Hg(1)−Te(1)	103.88(6)
S(2)−Hg(2)−S(1)	165.2(2)	Se(2)−Hg(2)−Se(1)	163.11(3)	Te(1)−Hg(2)−Te(2)	156.58(8)
Hg(2)−S(1)−Hg(1)	102.0(2)	Hg(2)−Se(1)−Hg(1)	101.35(3)	Hg(2)−Te(1)−Hg(1)	103.45(6)
Hg(2)−S(1)−Tl	85.31(15)	Hg(2)−Se(1)−Tl(1)	84.93(3)	Hg(2)−Te(1)−Tl	84.49(5)
Hg(1)−S(1)−Tl	125.9(2)	Hg(1)−Se(1)−Tl(1)	128.71(3)	Hg(1)−Te(1)−Tl	132.55(5)
Hg(2)−S(2)−Hg(1)	96.9(2)	Hg(2)−Se(2)−Hg(1)	94.52(3)	Hg(2)−Te(2)−Hg(1)	93.51(6)
Hg(2)−S(2)−Tl	97.93(17)	Hg(2)−Se(2)−Tl(1)	100.36(3)	Hg(2)−Te(2)−Tl	104.78(5)
Hg(1)−S(2)−Tl	112.8(2)	Hg(1)−Se(2)−Tl(1)	113.51(3)	Hg(1)−Te(2)−Tl	115.39(5)

[a] Estimated standard deviations are given in parentheses.

The X-ray intensity data of $Tl_2Hg_3Q_4$ were collected from single crystals at room temperature, using a STOE Model IPDS 2T diffractometer (with additional capability of 2θ swing of the detector) with graphite-monochromatized Mo Kα (λ = 0.71073 Å) radiation. The STOE X-AREA (X-RED and X-SHAPE within) package suite[38] was used for data extraction and integration, as well as to apply numerical absorption corrections. The structures were solved by direct methods and refined with the SHELXTL package of programs.[39] The room-temperature data give a stable refinement for all three compounds in the monoclinic space group $C2/c$. A total of five unique atomic positions were observed in the structure of $Tl_2Hg_3Q_4$. The Hg(1) atom resides at the 4*e* Wyckoff position and the Hg(2), Tl, Q(1), and Q(2) atoms reside at the 8*f* Wyckoff position. The details of the data collection and crystallographic refinement of $Tl_2Hg_3Q_4$ can be found in Table 1. A list of the atomic positions and the isotropic and anisotropic displacement parameters are given in Tables 2 and 3, and the bond distances and angles can be found in Tables 4 and 5, respectively.

Measurements of optical diffuse reflectance were performed at room temperature using a Shimadzu Model UV-3101PC double-beam, ultraviolet−visible light−near-infrared (UV-Vis-NIR) double monochromator spectrophotometer. Using the Kubelka−Munk function, $(1 - R)^2/2R$, where R is the reflectance, the band gaps can be found by extending a fit to the linear region to the intersection with the x-axis, as described previously.[40−43]

Density functional theory (DFT) band structure calculations were made using the full-potential linearized augmented plane wave (FLAPW) method[44] with the screened-exchange local density approximation (sx-LDA).[45] The core and valence states were treated fully and scalar relativistically, respectively. Experimental lattice parameters and atomic coordinates obtained in the single-crystal refinement reported here were used for the calculations. The energy cutoffs for the interstitial plane-wave basis and the star functions were 12.3 and 144 Ry, respectively.

RESULTS AND DISCUSSION

Synthesis, Crystal Growth, and Characterization. The crystals obtained were red, black, and gray metallic for the S, Se, and Te analogues, respectively, in agreement with the electronic absorption spectra discussed below. Specimens of $Tl_2Hg_3Se_4$ are shown in Figure 1. All samples are stable in air, although, when exposed to the atmosphere for months, they develop a bluish film on the surface.

Powder XRD patterns for ground crystals of all $Tl_2Hg_3Q_4$ compounds are shown in Figure 2. Calculated Bragg reflections from the refined crystal structures are also shown for comparison (red drop lines) and are in good agreement. The plate morphology resulting from the layered crystal structure gives rise to

dx.doi.org/10.1021/cm2019857 |Chem. Mater. 2011, 23, 4375–4383

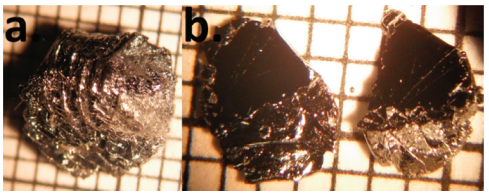

Figure 1. (a) $Tl_2Hg_3Se_4$ ingot obtained after removal of the Tl_xSe flux. (b) Cleaving of the ingot shown in panel (a) to expose mirrorlike surfaces.

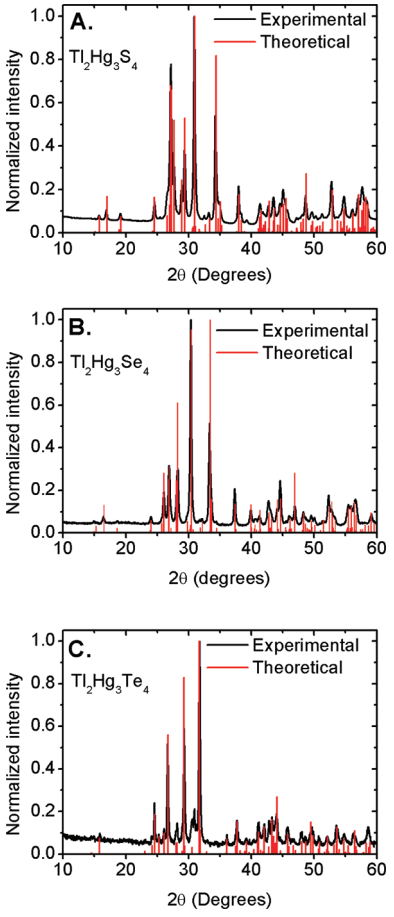

Figure 2. Powder X-ray diffraction (XRD) patterns for the (A) S, (B) Se, and (C) Te analogues. Bragg peaks from the structures, calculated based on the single-crystal refinements, are shown as red lines for comparison.

substantial preferred orientation, where Bragg peaks with (*hkl*) perpendicular to the [001] direction are attenuated while those aligned with the [001] are overly intense. This effect is more pronounced in the S and Se samples than in the Te sample, which could be a consequence of the increased covalency in the structure, resulting from the more-extended *p* states of Te atoms. This, in turns, leads to increased interlayer bonding and, consequently, less cleaving tendency along the layers. For the S and Te samples, the crystals obtained were all <1 mm^3, whereas the Se analogue precipitated in one single crystalline lump. The $Tl_2Hg_3Se_4$ sample was easily cleaved using a razor blade to obtain platelets with mirrorlike surfaces (see Figure 1). The generally smaller crystals of the S and Te analogues showed

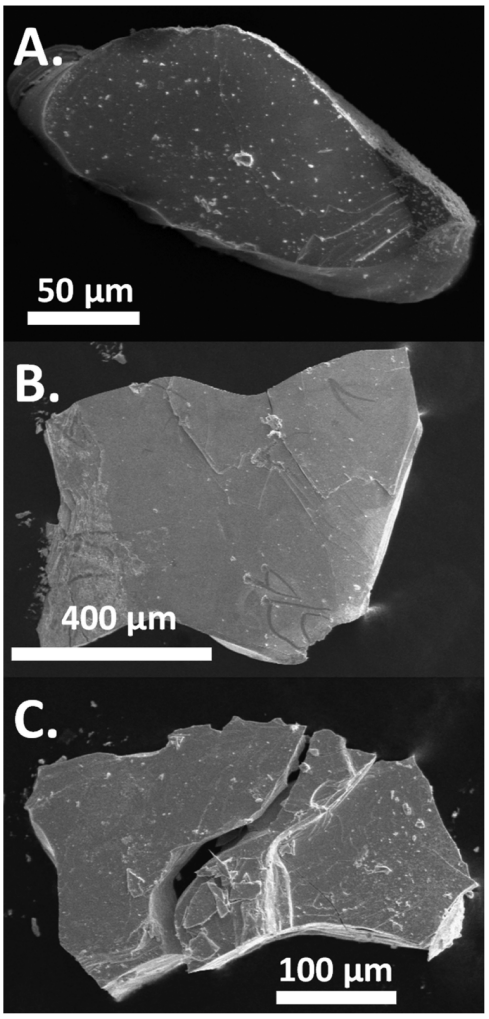

Figure 3. Scanning electron microscopy (SEM) images of selected $Tl_2Hg_3Q_4$ crystals: (A) S analogue, (B) Se analogue, and (C) Te analogue.

similar cleaving ability, which is again consistent with the layered crystal structures. The SEM images given in Figure 3 show typical platelike crystals, which is consistent with the layered crystal structure.

The low X-ray scattering contrast between Hg and Tl, as well as overlap of the characteristic X-ray fluorescent peaks of the two periodic table neighbors, can complicate the evaluation of the stoichiometry via XRD and EDS. Consequently, in addition to the flux method, samples were made with direct combination reactions to ensure that the stoichiometry is indeed $Tl_2Hg_3Q_4$. Powder XRD from these samples showed single phase purity, with the EDS stoichiometries matching those of the single crystals (see the Experimental Section and the Supporting Information).

Crystal Structure. The compounds of $Tl_2Hg_3Q_4$ (Q = S, Se, Te) are a subclass within a larger family of compounds with the general formula $A_2M_3Q_4$ (A = K, Rb, Cs; M = Mn, Co, Zn, Cd, Hg; and Q = S, Se, Te).[27,46−51] The Tl analogs crystallize in a distinct structure type. The alkali-metal analogues $A_2M_3Q_4$ crystallize in three different structure types: $K_2Cd_3S_4$-type (space group: *Pnma*), $Cs_2Zn_3S_4$-type (space group: *Ibam*), and $K_2Zn_3O_4$-type (space group: *C*2/*c*). However, $Tl_2Hg_3Q_4$ seems

dx.doi.org/10.1021/cm2019857 |*Chem. Mater.* 2011, 23, 4375–4383

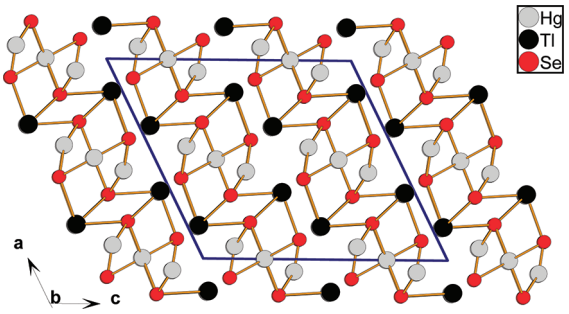

Figure 4. Crystal structure of $Tl_2Hg_3Se_4$ viewed along the *b*-axis. Interlayer Tl···Se interactions are omitted to highlight the layered character. The $[Hg_3Se_4]^{2-}$ chains are parallel to the *b*-axis.

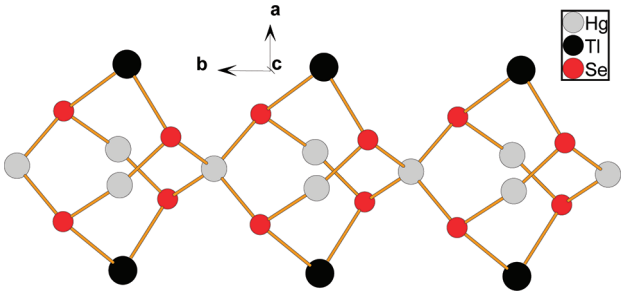

Figure 5. The chain structure of $[Hg_3Se_4]^{2-}$, which is comprised of tetrahedral and almost linear Hg atoms. The Tl atoms (represented by black solid circles) bond to the chains, forming $Tl_2Hg_3Se_4$ cages that extend along the *c*-direction.

to exhibit a new structure motif, shown in Figure 4. The crystal structure of $Tl_2Hg_3Q_4$ is built of Tl^+, Hg^{2+}, and Q^{2-} ions.

Depending on how the Tl^+ ions are viewed, the structure can be described in two alternative ways. If the Tl^+ ions are viewed strictly as counterions, similar to alkali-metal ions, then a saltlike description is $Tl^+_2[Hg_3Q_4]^{2-}$, where the covalent $[Hg_3Q_4]^{2-}$ part is a one-dimensional chain, similar to that found in $Cs_2Hg_3Se_4$.[32,52,53] If the covalent Tl−Q interactions are taken into account (they are significant, as indicated by our theoretical electronic band structure analysis below), then a layered covalent framework with the ternary composition $Tl_2Hg_3Q_4$ is a valid description.

In this latter view, the structure contains repeating "$Tl_2Hg_3Q_4$" cage-type units that are interconnected chains running along the *a*-axis direction. These chains then are arranged side by side and join with Tl−Q bonds to form a layered structure with the layers in the *ab* plane (see Figure 5). The layers themselves are separated by relatively short Tl···Q distances of 3.2482(6), 3.3864(6), and 3.3930(6) Å in $Tl_2Hg_3S_4$, $Tl_2Hg_3Se_4$, and $Tl_2Hg_3Te_4$, respectively.

Narducci et al.[50] made a generalization in the $A_2M_3Q_4$ family, based on their A:M ionic radius. The compounds that adopt the $K_2Cd_3S_4$ structure type have $1.77 \geq A{:}M \leq 1.95$ with 6-coordinate A atoms, whereas the $Cs_2Zn_3S_4$-type compounds have $A{:}M \geq 2.23$ with 8-coordinate A atoms. Compounds with the $K_2Zn_3O_4$ structure type lie between these two structure types. In $Tl_2Hg_3Q_4$, the Tl:Hg ionic radius ratio[54] of 1.24 is far below these values, which results in a distinct structure type. Although $Rb_2Cd_3Te_4$ also crystallizes in the same monoclinic $C2/c$ space group, its layered nature is

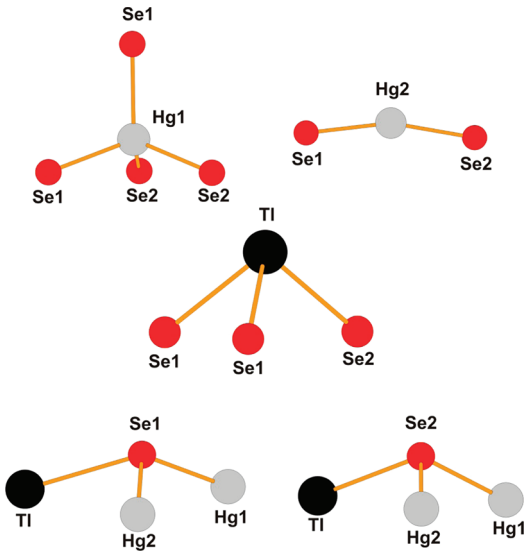

Figure 6. The local coordination of all crystallographically distinct atomic sites in $Tl_2Hg_3Se_4$.

due to the extended $[Cd_3Te_4]^{2-}$ layers, which are well-separated by Rb^+ ions.[50]

The coordination environment of each unique atom in the structure is shown in Figure 6. There are two types of Hg centers: tetrahedral and almost linear. Namely, Hg(1) forms a distorted tetrahedron with four long Hg−Q bonds, while Hg(2) is two-coordinated (see Table 2). The Q−Hg(2)−Q angle varies from 156.58(8)° to 163.11(3)° to 165.2(2)° from the Te, Se, and S analogues, respectively. This trend where the sulfide has the widest angle is somewhat surprising, because the cell volume decreases with chalcogen size. The tetra-coordinated Hg has previously been observed in $(Hg_3Te_4)^{2-}$,[51] $(Hg_4Te_{12})^{4-}$,[55] $[Hg_3Te_7]^{4-}$,[56] and $(HgTe_8)^{2-}$,[57] while the bicoordinated Hg has been observed in the $A_2Hg_3Q_4$ family.[32,51−53] The relatively large thermal parameters for Hg(2) in $Tl_2Hg_3Te_4$ can be explained by the two-coordinate geometry of the Hg(2) environment.

The Q atoms have trigonal-pyramidal coordination with two Hg atoms and one Tl atom. This type of coordination is common in the $A_2Hg_3Q_4$ family.[32,51−53] From the coordination of Tl (see Figure 6), it is evident that the so-called inert lone pair of electrons is accommodated in the interlayer spaces and plays a large role in defining the overall structure. This makes $Tl_2Hg_3Q_4$ fundamentally different from the rest of the $A_2Hg_3Q_4$ family,[32,51−53] where the ionic alkali elements are found within the interlayer gap. In order to accommodate the Tl^+ inert lone pair, the structure is distorted to create pockets between the layers.

ELECTRONIC STRUCTURE AND ENERGY BAND GAPS

It is well-known that, in DFT calculations using local density approximation (LDA), the band gap is almost always underestimated and only the calculated relative trend among isostructural chalcogen compounds is consistent with the experimental observations.[58,59] The present study confirms this: the band gaps calculated with simple LDA are 0.71−0.75 eV below the experimentally observed band gaps (see the Supporting Information). However, application of the sx-LDA method yields

dx.doi.org/10.1021/cm2019857 |*Chem. Mater.* 2011, 23, 4375–4383

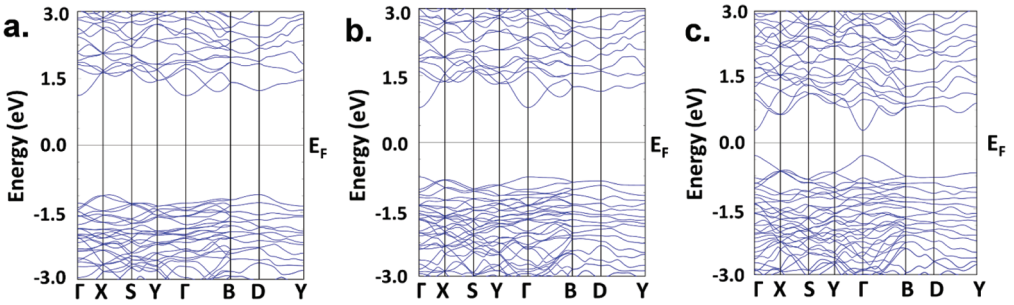

Figure 7. Calculated band structures for the $Tl_2Hg_3Q_4$ samples ((a) Q = S, (b) Q = Se, and (c) for Q = Te).

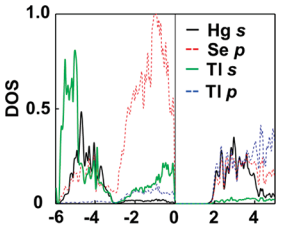

Figure 8. Calculated density of states (in units of states per eV per unit cell) for $Tl_2Hg_3Se_4$ with specified atomic orbital contributions.

band gaps that are in good agreement with the experimentally observed values.[8,60−64] The sx-LDA electronic band structures for all compounds of the $Tl_2Hg_3Q_4$ family are shown in Figure 7. They reveal that these are semiconductors with a narrow valence band, a relatively broad conduction band, and wide energy band gaps. The *p* states of the chalcogen atoms strongly contribute to both the valence band maximum (VBM) and the conduction band minimum (CBM), as seen in Figure 8. This has serious implications on the band structure near the Fermi level. As the *p* states become more extended, there is a marked decrease in the calculated band gap, which decreases from 2.22 eV in the S sample to 1.56 eV in the Se sample and to 0.57 eV in the Te sample. This is a consequence of increasing the energy dispersion from enhanced orbital overlap. Furthermore, there is a profound change in the nature of the band gap. The gap, which is indirect from D−Γ in the S analog, becomes direct, Γ−Γ, in both the Se and Te analogues.

Finally, because of the increased band dispersion, the effective mass of the charge carriers is reduced in going from the S compound to the Se compound to the Te compound. Aside from the predominantly chalcogen *p* state character, there is a substantial contribution from Tl 6*s* states to the VBM, while the CBM has a pronounced Hg 6*s* state character. Since Hg 6*s* states are extended and of isotropic character, the dispersion of the conduction band is parabolic and isotropic, and has a relatively large bandwidth, compared to that of the valence bands. Consequently, the effective masses of the *n*-type carriers are small relative to the *p*-type carriers, resulting in high *n*-type carrier mobility. Therefore, these compounds may be promising for applications where a wide band gap and high mobility are key requirements (e.g., X-ray and γ-ray detection).[14,34] An exception to this is $Tl_2Hg_3Te_4$; for this compound, the calculations indicate that its valence band has significant dispersion. In this case, the hole carriers should have higher mobilities than the S and Se analogues.

Optical Spectroscopy. The solid-state optical spectra confirm the increase in band gap, resulting from the addition of

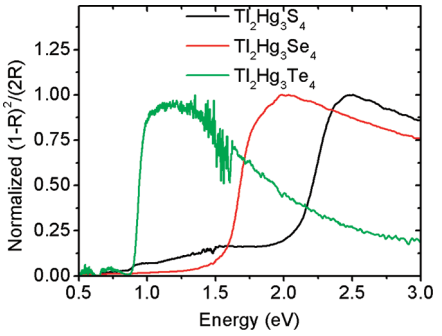

Figure 9. Electronic absorption spectra recorded for ground $Tl_2Hg_3Q_4$ crystals.

Tl_2Q to the HgQ structure to form $Tl_2Hg_3Q_4$. Comparison of the band gaps of $Tl_2Hg_3Q_4$ with HgQ reveals the effects of DR. Namely, HgQ in the zincblende structure has band gaps of 0, −0.06, and −0.14 eV for S, Se, and Te, respectively,[33] while the lower-dimensional structure of $Tl_2Hg_3Q_4$ results in a marked increase in the band gaps, to 2.05(4), 1.57(2), and 0.90(1) eV for the S, Se, and Te compounds, respectively (see Figure 9). The increase in orbital extent of the outermost *s* and *p* orbitals of the chalcogen atoms in the series S, Se, and Te accounts for the systematic decrease in band gap observed, as discussed in the band structure analysis above. Because of their isostructural nature, the $Tl_2Hg_3Q_4$ compounds are likely to form solid solutions, which should permit band-gap engineering (e.g., $Tl_2Hg_3Q_{4-x}Q'_x$), as well as chemical tuning of the gap from indirect to direct.

It would be interesting to compare the band gaps of the Tl and alkali-metal analogues that contain the same $[Hg_3Q_4]^{2-}$ moiety. Among the latter, we have measured $K_2Hg_3S_4$ and $K_2Hg_3Se_4$ to have band gaps of ∼2.6 and 2.2 eV, respectively. These are larger than the $Tl_2Hg_3Q_4$ compounds, by more than 0.5 eV. Hence, although the A···Q bonds are largely ionic in nature, the Tl···Q bonds exhibit considerable covalency, which results in further band broadening and a narrowing of the band gap. This is supported by the band structure calculations, which reveal a considerable Tl 6*s* and 6*p* character of both the VBM and CBM.

■ CONCLUDING REMARKS

The incongruently melting compounds $Tl_2Hg_3Q_4$ (Q = S, Se, and Te) were synthesized as single crystals in a Tl_xQ flux, as well as in polycrystalline form, via direct combination. Their structures and electronic properties can be understood within the "dimensional reduction" (DR) concept. The extra Q^{2-} ions

dx.doi.org/10.1021/cm2019857 |*Chem. Mater.* 2011, 23, 4375–4383

inserted into the three-dimensional (3D) HgQ structure cleave bonds to form a one-dimensional (1D) $[Hg_3Q_4]^{2-}$ chain, while bonding interactions of electropositive Tl atoms and the formation of covalent Tl−Q bonds gives rise to an overall two-dimensional (2D) $Tl_2Hg_3Q_4$ structure. Hence, the materials can be viewed as layered slabs of "$Tl_2Hg_3Q_4$" interconnected by weak Tl···Q bonds and van der Waal forces. This is reflected in the electronic absorption spectra, where the band gaps increase from 0 eV for HgQ to 0.90−2.05 eV for $Tl_2Hg_3Q_4$ (as Q goes from Te to S). The density functional theory (DFT) screened-exchange local density approximation (sx-LDA) band structure calculations confirm the covalent Tl···Q interactions, as well as the concomitant narrowing of the band gap as the chalcogen *p*-states become more extended in going from S to Te. The calculations indicate that the conduction band minimum (CBM) is highly dispersed relative to the valence band maximum (VBM), indicative of significantly different transport properties for holes and electrons, with high *n*-type carrier mobility. The $Tl_2Hg_3Q_4$ compounds are expected to be highly absorbing of hard radiation, because of their very high mass density (>8.3 g/cm^3) resulting from the dense crystal packing and heavy elements. In addition, the S and Se analogues have wide band gaps, as indicated by optical measurements. For these reasons, the $Tl_2Hg_3Q_4$ compounds show great potential as X-ray and γ-ray detector materials, which are required to be highly dense, wide-band-gap semiconductors (>1.5 eV) with high mobilities. For example, we have recently shown that another thallium chalcogenide compound, $TlGaSe_2$, can exhibit promising X-ray detection properties.[65] The isostructural nature of the $Tl_2Hg_3Q_4$ compounds suggests that solid-solution formation by mixing chalcogens can be used to engineer band structures and band-gap energies for optoelectronic applications.

■ ASSOCIATED CONTENT

Supporting Information. Figures S1−S3 show powder diffraction patterns for the $Tl_2Hg_3Q_4$ samples synthesized via direct combination. Figure S4 shows band structures for $Tl_2Hg_3Q_4$ calculated using LDA. CIF files for $Tl_2Hg_3S_4$, $Tl_2Hg_3Se_4$, and $Tl_2Hg_3Te_4$ are also provided. This material is available free of charge via the Internet at http://pubs.acs.org.

■ AUTHOR INFORMATION

Corresponding Author

*E-mail: m-kanatzidis@northwestern.edu.

Present Addresses

[▽]New Chemistry Unit, Jawaharlal Nehru Centre for Advanced Scientific Research, Jakkur, Bangalore 560064, India.

■ ACKNOWLEDGMENT

S.J. would like to acknowledge the Danish Research Council for Nature and Universe for funding. This work is supported by a Department of Homeland Security grant (ARI-MA: 2010-DN-077-ARI042-02).

■ DEDICATION

[†]Dedicated in memory of Dr. Jung-Hwan Song.

■ REFERENCES

(1) Todorov, T. K.; Reuter, K. B.; Mitzi, D. B. *Adv. Mater.* **2010**, *22*, E156–E159.
(2) Britt, J.; Ferekides, C. *Appl. Phys. Lett.* **1993**, *62*, 2851–2852.
(3) Repins, I.; Contreras, M. A.; Egaas, B.; DeHart, C.; Scharf, J.; Perkins, C. L.; To, B.; Noufi, R. *Prog. Photovolt.* **2008**, *16*, 235–239.
(4) Androulakis, J.; Lin, C. H.; Kong, H. J.; Uher, C.; Wu, C. I.; Hogan, T.; Cook, B. A.; Caillat, T.; Paraskevopoulos, K. M.; Kanatzidis, M. G. *J. Am. Chem. Soc.* **2007**, *129*, 9780–9788.
(5) Hsu, K. F.; Loo, S.; Guo, F.; Chen, W.; Dyck, J. S.; Uher, C.; Hogan, T.; Polychroniadis, E. K.; Kanatzidis, M. G. *Science* **2004**, *303*, 818–821.
(6) Sootsman, J. R.; Kong, H.; Uher, C.; D'Angelo, J. J.; Wu, C. I.; Hogan, T. P.; Caillat, T.; Kanatzidis, M. G. *Angew. Chem., Int. Ed.* **2008**, *47*, 8618–8622.
(7) Biswas, K.; He, J.; Zhang, Q.; Wang, G.; Uher, C.; Dravid, V. P.; Kanatzidis, M. G. *Nat. Chem.* **2011**, *3*, 160–166.
(8) Bera, T. K.; Jang, J. I.; Song, J. H.; Malliakas, C. D.; Freeman, A. J.; Ketterson, J. B.; Kanatzidis, M. G. *J. Am. Chem. Soc.* **2010**, *132*, 3484–3495.
(9) Bera, T. K.; Jang, J. I.; Ketterson, J. B.; Kanatzidis, M. G. *J. Am. Chem. Soc.* **2009**, *131*, 75–77.
(10) Liao, J. H.; Marking, G. M.; Hsu, K. F.; Matsushita, Y.; Ewbank, M. D.; Borwick, R.; Cunningham, P.; Rosker, M. J.; Kanatzidis, M. G. *J. Am. Chem. Soc.* **2003**, *125*, 9484–9493.
(11) Bordui, P. F.; Fejer, M. M. *Ann. Rev. Mater. Sci.* **1993**, *23*, 321–379.
(12) Hegedus, J.; Elliott, S. R. *Nat. Mater.* **2008**, *7*, 399–405.
(13) Pirovano, A.; Lacaita, A. L.; Benvenuti, A.; Pellizzer, F.; Bez, R. *IEEE Trans. Electron Devices* **2004**, *51*, 452–459.
(14) Owens, A. *J. Synchrotron Radiat.* **2006**, *13*, 143–150.
(15) MacKenzie, J.; Chen, H.; Awadalla, S. A.; Marthandam, P.; Redden, R.; Bindley, G.; He, Z.; Black, D. R.; Duff, M.; Amman, M.; Lee, J. S.; Luke, P. N.; Groza, M.; Burger, A. Recent advances in THM CZT for Nuclear Radiation Detection. In *Nuclear Radiation Detection Materials—2009*, Fiederle, M., Perry, D. L., Burger, A., Franks, L., Yasuda, K., Eds.; Materials Research Society: Warrendale, PA, 2010; Vol. 1164, pp 155−164.
(16) Manos, M. J.; Chrissafis, K.; Kanatzidis, M. G. *J. Am. Chem. Soc.* **2006**, *128*, 8875–8883.
(17) Manos, M. J.; Ding, N.; Kanatzidis, M. G. *Proc. Natl. Acad. Sci. U.S.A.* **2008**, *105*, 3696–3699.
(18) Manos, M. J.; Kanatzidis, M. G. *Chem.—Eur. J.* **2009**, *15*, 4779–4784.
(19) Manos, M. J.; Kanatzidis, M. G. *J. Am. Chem. Soc.* **2009**, *131*, 6599–6607.
(20) Manos, M. J.; Petkov, V. G.; Kanatzidis, M. G. *Adv. Funct. Mater.* **2009**, *19*, 1087–1092.
(21) Zhang, H. J.; Liu, C. X.; Qi, X. L.; Dai, X.; Fang, Z.; Zhang, S. C. *Nat. Phys.* **2009**, *5*, 438–442.
(22) Jin, H. S.; Song, J. H.; Freeman, A. J.; Kanatzidis, M. G. *Phys. Rev. B* **2011**, *83*, 041202.
(23) Urazhdin, S.; Bilc, D.; Mahanti, S. D.; Tessmer, S. H.; Kyratsi, T.; Kanatzidis, M. G. *Phys. Rev. B* **2004**, *69*, 085313.
(24) Hasan, M. Z.; Kane, C. L. *Rev. Mod. Phys.* **2010**, *82*, 3045–3067.
(25) Tulsky, E. G.; Long, J. R. *Chem. Mater.* **2001**, *13*, 1149–1166.
(26) Axtell, E. A.; Park, Y.; Chondroudis, K.; Kanatzidis, M. G. *J. Am. Chem. Soc.* **1998**, *120*, 124–136.
(27) Axtell, E. A.; Liao, J. H.; Pikramenou, Z.; Kanatzidis, M. G. *Chem.—Eur. J.* **1996**, *2*, 656–666.
(28) (a) Evenson, C. R.; Dorhout, P. K. *Inorg. Chem.* **2001**, *40*, 2884–2891. (b) Chondroudis, K.; McCarthy, T. J.; Kanatzidis, M. G. *Inorg. Chem.* **1996**, *35*, 840. (c) Liao, J. H.; Kanatzidis, M. G. *Chem. Mater.* **1993**, *5*, 1561. (d) McCarthy, T. J.; Kanatzidis, M. G. *Inorg. Chem.* **1995**, *34*, 1257.
(29) Rumpf, C.; Tillinski, R.; Nather, C.; Durichen, P.; Jess, I.; Bensch, W. *Eur. J. Solid State Inorg. Chem.* **1997**, *34*, 1187–1198.
(30) Lekse, J. W.; Moreau, M. A.; McNerny, K. L.; Yeon, J.; Halasyamani, P. S.; Aitken, J. A. *Inorg. Chem.* **2009**, *48*, 7516–7518.

(31) Axtell, E. A.; Liao, J. H.; Pikramenou, Z.; Park, Y. B.; Kanatzidis, M. G. *J. Am. Chem. Soc.* **1993**, *115*, 12191–12192.
(32) Kanatzidis, M. G.; Park, Y. *Chem. Mater.* **1990**, *2*, 99–101.
(33) Madelung, O., *Semiconductors: Data Handbook*, 3rd ed.; Springer: Berlin, 2004.
(34) Milbrath, B. D.; Peurrung, A. J.; Bliss, M.; Weber, W. J. *J. Mater. Res.* **2008**, *23*, 2561–2581.
(35) Asadov, M. M.; Babanly, M. B.; Kuliev, A. A. *Z. Neorg. Khimii* **1982**, *27*, 3173–3178.
(36) Babanly, M. B.; Asadov, M. M.; Kuliev, A. A. *Inorg. Mater.* **1983**, *19*, 524–528.
(37) Kuliev, A. A.; Asadov, M. M.; Kuliev, R. A.; Babanly, M. B. *Z. Neorg. Khimii* **1978**, *23*, 854–856.
(38) *STOE*; Cie STOE & Cie GmbH: Darmstadt, Germany, 2006.
(39) Sheldrick, G. M. *SHELXS-97, Program for the Solution of Crystal Structure*; University of Göttingen: Göttingen, Germany, 1997.
(40) Tandon, S. P.; Gupta, J. P. *Phys. Status Solidi* **1970**, *38*, 363–367.
(41) Bag, S.; Trikalitis, P. N.; Chupas, P. J.; Armatas, G. S.; Kanatzidis, M. G. *Science* **2007**, *317*, 490–493.
(42) Liao, J. H.; Kanatzidis, M. G. *Chem. Mater.* **1993**, *5*, 1561–1569.
(43) Trikalitis, P. N.; Rangan, K. K.; Bakas, T.; Kanatzidis, M. G. *J. Am. Chem. Soc.* **2002**, *124*, 12255–12260.
(44) Wimmer, E.; Krakauer, H.; Weinert, M.; Freeman, A. J. *Phys. Rev. B* **1981**, *24*, 864–875.
(45) Rhim, S. H.; Kim, M.; Freeman, A. J.; Asahi, R. *Phys. Rev. B* **2005**, *71*, 045202.
(46) Bronger, W.; Hendriks, U.; Muller, P. *Z. Anorg. Allg. Chem.* **1988**, *559*, 95–105.
(47) Bronger, W.; Hardtdegen, H.; Kanert, M.; Muller, P.; Schmitz, D. *Z. Anorg. Allg. Chem.* **1996**, *622*, 313–318.
(48) Wu, E. J.; Ibers, J. A. *Acta Crystallogr., Sect. C: Cryst. Struct. Commun.* **1997**, *53*, 993–994.
(49) Baier, R.; Hoppe, R. *Z. Anorg. Allg. Chem.* **1987**, *551*, 163–172.
(50) Narducci, A. A.; Ibers, J. A. *J. Alloys Compd.* **2000**, *306*, 170–174.
(51) Li, J.; Chen, Z.; Lam, K. C.; Mulley, S.; Proserpio, D. M. *Inorg. Chem.* **1997**, *36*, 684–687.
(52) Kanatzidis, M. G.; Sutorik, A. C. *Prog. Inorg. Chem.* **1995**, *43*, 151–265.
(53) Klepp, K. O. *J. Alloys Compd.* **1992**, *182*, 281–288.
(54) Shannon, R. D. *Acta Crystallogr., Sect. A: Cryst. Phys., Diffr., Theor. Gen. Crystallogr.* **1976**, *32*, 751–767.
(55) Haushalter, R. C. *Angew. Chem., Int. Ed.* **1985**, *24*, 433–435.
(56) Dhingra, S. S.; Warren, C. J.; Haushalter, R. C.; Bocarsly, A. B. *Chem. Mater.* **1994**, *6*, 2382–2385.
(57) Bollinger, J. C.; Roof, L. C.; Smith, D. M.; Mcconnachie, J. M.; Ibers, J. A. *Inorg. Chem.* **1995**, *34*, 1430–1434.
(58) Asahi, R.; Mannstadt, W.; Freeman, A. J. *Phys. Rev. B* **2000**, *62*, 2552–2561.
(59) Stampfl, C.; Asahi, R.; Freeman, A. J. *Phys. Rev. B* **2002**, *65*, 161204.
(60) Bera, T. K.; Song, J. H.; Freeman, A. J.; Jang, J. I.; Ketterson, J. B.; Kanatzidis, M. G. *Angew. Chem., Int. Ed.* **2008**, *47*, 7828–7832.
(61) Biswas, K.; Zhang, Q. C.; Chung, I.; Song, J. H.; Androulakis, J.; Freeman, A. J.; Kanatzidis, M. G. *J. Am. Chem. Soc.* **2010**, *132*, 14760–14762.
(62) Chung, I.; Song, J. H.; Jang, J. I.; Freeman, A. J.; Ketterson, J. B.; Kanatzidis, M. G. *J. Am. Chem. Soc.* **2009**, *131*, 2647–2656.
(63) Tsamourtzi, K.; Song, J. H.; Bakas, T.; Freeman, A. J.; Trikalitis, P. N.; Kanatzidis, M. G. *Inorg. Chem.* **2008**, *47*, 11920–11929.
(64) Ye, L. H.; Hoang, K.; Freeman, A. J.; Mahanti, S. D.; He, J.; Tritt, T. M.; Kanatzidis, M. G. *Phys. Rev. B* **2008**, *77*, 245203.
(65) Johnsen, S.; Liu, Z.; Peters, J. A.; Song, J.-H.; Peter, S. C.; Malliakas, C. D.; Cho, N. K.; Jin, H.; Freeman, A. J.; Wessels, B. W.; Kanatzidis, M. G. *Chem. Mater.* **2011**, *23*, 3120–3128.